Astron. Astrophys. 346, 441–452 (1999)

ASTRONOMY AND ASTROPHYSICS

The circumstellar environment of IRAS 05327+3404

E.A. Magnier[1,2], L.B.F.M. Waters[1,3], P.J. Groot[1], M.E. van den Ancker[1], Y.-J. Kuan[4,5], and E.L. Martín[6,7]

[1] Astronomical Institute "Anton Pannekoek" and CHEAF, Kruislaan 403, 198 SJ Amsterdam, The Netherlands
[2] Astronomy Dept. 351580, University of Washington, Seattle, WA 98195, USA
[3] SRON Laboratory for Space Research Groningen, P.O. Box 800, 9700 AV Groningen, The Netherlands
[4] Department of Earth Sciences, National Taiwan Normal University, Taipei, Taiwan
[5] Institute of Astronomy and Astrophysics, Academia Sinica, P.O. Box 1-87, Nankang, Taipei, Taiwan
[6] Instituto de Astrofísica de Canarias, E-38200 La Laguna, Tenerife, Spain
[7] Astronomy Dept., 601 Campbell Hall, University of California at Berkeley, CA 94720, USA

Received 20 February 1998 / Accepted 21 August 1998

Abstract. We continue our study of the young stellar object associated with IRAS 05327+3404. We have determined the spectral type of the central star to be K2. We show that the star is most likely seen directly, not via a reflection, and that the extinction is only $A_V \sim 2.3$ mag. The spectral energy distribution shows the presence of large amounts of circumstellar material. Near-IR and optical observations of the reflection nebula also demonstrate the presence of circumstellar material, and show the material to be arranged in a disk with a relatively wide central hole of $\sim 33^\circ$ opening angle. The central hole and a CO outflow are co-aligned, and are roughly aligned with the ionized outflow. Several surprising aspects remain: Although the system has a strong ionized outflow, there is little or no evidence of active accretion in the form of UV excess, veiling, or strong high-Balmer line emission. Also, the spectral energy distribution is very wide, and suggests that the original birth cloud had a large rotational velocity. We propose that the relative isolation of the system from other star formation activity may explain the relatively large circumstellar disk for a system with a well-exposed central star.

Key words: stars: circumstellar matter – stars: evolution – stars: formation – stars: mass-loss – stars: pre-main sequence

1. Introduction

A major problem in the study of the early stages of star formation is the fact that they are obscured by large amounts of circumstellar dust, making them invisible at optical wavelengths. By observing at longer wavelengths, we can study more obscured, and thus generally younger, sources but at these wavelengths we are looking more at the circumstellar material than the photosphere of the protostar itself. Choosing only the less obscured stars selects older objects. Only a few sources are known which show features of the young, embedded systems, but which are visible in the optical or the near IR. The flat spectrum sources, at the boundary between the Class I and Class II systems, are thought to be close to this transition.

We are studying a young star which is an excellent example of an object close to the Class I / Class II boundary. This transitional Young Stellar Object (YSO), which is associated with IRAS 05327+3404, was first discussed by Magnier et al. (1996; Paper I). We refer to the outflow source by the nickname "Holoea" because of the unusually powerful ionized outflow (see Paper I) and to distinguish it from the other, weaker sources of far-IR emission in the vicinity. In Paper I, we showed that IRAS 05327+3404 (Holoea) has some features typical of Class I sources (rising spectral energy distribution, molecular bipolar outflow) and some features typical of Class II sources (visible central star, ionized outflow). Furthermore, the outflow is of an unusually high velocity ($\sim$650 km s^{-1}) for a low-mass star (roughly K2), and the central star has brightened by > 1.5 magnitudes since the 1954 POSS plates. All of these pieces of evidence suggest that this source is not only close to the Class I / Class II (Lada & Wilking 1984) boundary, but in fact in the process of becoming exposed. We are continuing the study of this transitional YSO to gain further understanding of this short-lived stage of stellar evolution. We have recently obtained new observations from optical to sub-millimeter wavelengths. In this paper, we discuss the implications of these new data on our understanding of the circumstellar material and the reflection nebula of IRAS 05327+3404 (Holoea).

2. Observations

In this paper we report on the results of several new sets of observations. The new observations include: CO J=2-1 mapping and sub-mm continuum photometry with the James Clerk Maxwell Telescope, near IR wide-band images taken with the United Kingdom Infrared Telescope, and optical spectroscopy obtained at the Isaac Newton Telescope.

Send offprint requests to: Eugene A. Magnier
Correspondence to: gene@astro.uva.nl

2.1. JCMT observations

Observations of IRAS 05327+3404 in the submillimeter regime were made with the 15m James Clerk Maxwell Telescope (JCMT) on Mauna Kea in the fall of 1995. Both continuum and line observations were made. The observations were performed by the on-site staff, with the authors in remote contact. Continuum observations were made at 350, 450, 800 and 1100 μm using the UKT14 receiver. For each of the bands, the position of the optical star was observed with an aperture of 65 mm, which corresponds to 18.″2 at 1100μm and roughly 16.″5 at the three other wavelengths. Sky subtraction was performed with chopping every 16 seconds. Photometric measurements were made at 800 and 1100 μm data on Aug 24, 1995 using W3(OH), GL 490 and NGC 2071IR as calibration sources. The night was not photometric, and the opacity varied during the observations, so that the calibration is uncertain at the level of $\sim$10%. Observations at 800 μm were also performed using the 47mm aperture (13.″2 beam). The comparison of the two 800 μm observations suggests that the source may be slightly extended at these wavelengths, though the difference could be the result of calibration errors. Observations were performed at 350, 450, and 800 μm on Aug 26, 1995 when the sky transparency was significantly better. Calibration was performed with GL 490. The second observation at 800 μm with the 65mm aperture was significantly different from the first, suggesting some 15% calibration error the first night. The measured flux densities are listed in Table 1, which includes only the 800 μm flux from the second (better) of the two nights.

In addition to the continuum observations, a raster-map of a large region surrounding IRAS 05327+3404 (Holoea) was made of the CO J=2-1 transition. These line observations were observed using the Digital Autocorrelating Spectrometer with the On-The-Fly mapping mode. The CO J=2-1 beam size of the JCMT is $\sim$20″. We imaged a $100'' \times 250''$ region, which was fully sampled with 10″ grid spacing in RA and 5″ in Dec.

2.2. UKIRT observations

Observations of Holoea were made with the 3.8m United Kingdom Infrared Telescope (UKIRT) on Mauna Kea. The observations were made as part of the Service Time program, during the night of November 20, 1995. The weather during the night was photometric. Observations were made with IRCAM3, a near-IR imaging camera which uses a 256×256 InSb array. The pixel scale of the array is roughly 0.″28. Observations were taken with each of the three wide filters J, H, and K, and the narrow continuum filter nbL (similar to L' but narrower). UKIRT Faint Standards FS 12 and FS 15 (Casali & Hawarden 1992) were used as standards for the J, H, and K observations, while HD 40335 was used as a standard to convert the nbL photometry to L' magnitudes. For each filter, a series of offset images were taken and mosaicked together. IRCAM3 allows for on-chip averaging of series of exposures, avoiding problems with the limited well depth compared to the high background typical in IR observations. The total effective exposure time in each filter is listed in Table 1. Image pre-processing (flat-fielding and mosaicking) were performed by the UKIRT staff.

Table 1. Photometry data for IRAS 05327+3404 (Holoea)

band	mag	mJy	telescope	time
B	$>$20.00	$<$0.04 [1]	MDM[4] 1.3m	100 s
V	18.74 ± 0.05	0.116 ± 0.006 [1]	MDM[4] 1.3m	100 s
R	17.54 ± 0.03	0.297 ± 0.009 [1]	NOT 2.5m	30 s
I	16.36 ± 0.03	0.78 ± 0.02 [1]	NOT 2.5m	30 s
J	13.66 ± 0.03	5.5 ± 0.2 [1]	UKIRT 3.8m	540 s
H	12.73 ± 0.04	8.3 ± 0.3 [1]	UKIRT 3.8m	540 s
K	11.77 ± 0.05	13.2 ± 0.7 [1]	UKIRT 3.8m	540 s
nbL	7.91 ± 0.05	199 ± 10	UKIRT 3.8m	480 s
12 μm	–	870 ± 130	IRAS	–
25 μm	–	2610 ± 390	IRAS	–
60 μm	–	10680 ± 1600	IRAS	–
100 μm	–	15950 ± 2400	IRAS	–
350 μm	–	2640 ± 360 [2]	JCMT 15m	3200 s
450 μm	–	2070 ± 270 [2]	JCMT 15m	2240 s
800 μm	–	293 ± 19 [2,3]	JCMT 15m	480 s
1100 μm	–	129 ± 12 [2]	JCMT 15m	960 s

[1] optical, near-IR fluxes exclude reflection nebula
[2] JCMT errors don't include uncertainty in calibration sources
[3] 800 μm data show evidence of extended emission
[4] Michigan-Dartmouth-MIT Observatory

The central source in the J, H, and K images is roughly stellar but it is surrounded by extended emission which makes photometry difficult. We used a template point spread function made by averaging several nearby stars to make a better determination of the photometry of the central stellar source. The template was scaled and subtracted from the image of Holoea. The scaling of the template was chosen to minimize the amplitude of the residuals. This process was done by eye because some of the residual emission is due to real extended emission, so some judgement had to be made as to the correct amount of residual to leave behind. The J, H, K, and nbL photometry of the central source are listed in Table 1. The errors in the J, H, and K photometry are dominated by the uncertainty in remaining real extended emission after the template was subtracted. The nbL photometric errors are dominated by calibration error since there is no evidence of extended emission in these images.

2.3. NOT observations

Two images were obtained at the 2.5m Nordic Optical Telescope (NOT) November 8, 1994 using R and I filters. These images have been reported in Paper I. We have made improved photometric calibrations of these images using observations in R and I taken in September 1993. As with the *J, H, K* images, the central source is roughly stellar but surrounded by extended emission. We used the technique described above to fit a stellar profile to the central source. The resulting R and I photometry is listed in Table 1. We have also listed improved photometry for the central source in B and V from images taken in September 1993 and discussed in Paper I.

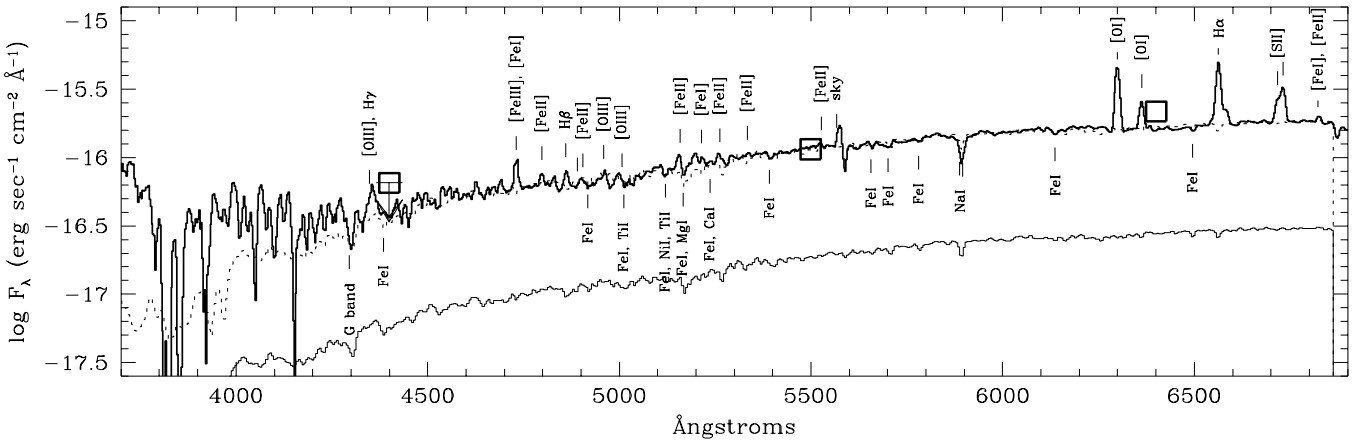

Fig. 1. Low resolution spectrum (thick line) with K2 III template spectrum (dotted line; Silva & Cornell 1992). The template is also shown offset for clarity (thin line). The boxes are wide-band B, V, and R photometry (upper limit for B).

2.4. INT observations

Low-resolution spectra of Holoea were obtained using the 2.5m Isaac Newton Telescope (INT) at the Observatorio de Roque de los Muchachos, La Palma. These observations were taken on 27 March, 1996 using the low resolution R300V grating on the IDS spectrograph. The projected pixel size is 0.″7. We used a wide (3.″25) slit to get as much light of Holoea as possible. This gives us a wavelength resolution of ∼5Å. Total on-target integration time was one hour. The orientation of the slit was North-South, i.e. along the optical tail. The spectrum of the star was extracted from the inner 4″ centered on the star, where the stellar flux dominates the extended emission. The visible extent of the tail was 15.″5. The data have been bias subtracted and flat-fielded in the standard way, using the ESO MIDAS reduction program. Wavelength calibration was done using a CuAr calibration spectrum. The resulting tail and star spectrum were flux calibrated using the spectrophotometric standard star Feige 34 (Massey et al. 1988). A spectrum with less exposure time was also obtained a year earlier, on March 17, 1995. No significant variation is seen between the two spectra.

3. The central source

In Paper I, we determined the spectral type of the central star to be roughly early K on the basis of a high resolution spectrum in the range 6100Å to 6800Å. We have now used our low resolution spectrum to make a better determination of the spectral type as well as the amount of extinction and veiling present in the system. Fig. 1 shows the measured spectrum with our calibrated B, V, R observations shown as squares. The excellent correspondence between the broadband fluxes and the spectrum shows our spectrophotometry is well calibrated.

We have labeled and identified the significant emission and absorption lines visible in this spectrum. Metal absorption lines typical of late-type stars and emission lines typical of T Tauri stars (Balmer and various forbidden lines) are clearly present, while strong molecular bands are absent.

Table 2. Spectral class comparisons

Type	A_V	Q	Type	A_V	Q	Type	A_V	Q
F7 I	2.5	2	G5-6 III	3.2	2	G6-8 V	3.3	2
G0-1 I	3.0	2	G8-K0 III	2.7	1	G9-K0 V	3.2	1
K1-2 I	2.2	1	K2 III	2.3	1	K4 V	2.5	3
K3-5 I	1.2	3	K4 III	1.5	2	K5 V	2.0	2
Q = Quality: 1 = best; 2 = middle; 3 = worst								

3.1. Spectral type and veiling

We compared our spectrum to the template spectra of Silva & Cornell (1992) available in electronic form. The strength of the Fe I absorption lines in the region 4900Å to 6500Å implies the spectral type cannot be earlier than ∼G6. Conversely, the absence of strong TiO bands at 5170Å and 6160Å constrains the spectral type to be earlier than ∼K5. The TiO band at 5170Å may be weakly present, suggesting a best spectral type of ∼K1. The high-luminosity models are also more favored because of the weakness of the bands given the strength of the absorption lines. The K2 III and G8-K0 III spectra give the best comparison, though the K1-2 I and G9-K0 V spectra compare almost as well. Table 2 lists our assessments of a range of models including these four and several other, less likely spectral types.

In our comparisons with the template spectra, we principally used the strength of the absorption lines and bands to constrain the spectral type. It is also possible to use the general shape of the spectrum to constrain the extinction, as well as other effects. We applied the standard extinction curve, tabulated by Whittet (1992), to the template spectra, and determined the best value of A_V for each spectral type. These extinction values are also given in Table 2. Fig. 1 includes the best-fit spectral template (K2 III), adjusted for 2.3 magnitudes of extinction.

There are several other effects in addition to the extinction which can change the continuum shape. First, the extinction may not follow the standard Galactic extinction curve, and may instead be anomalous. Anomalous extinction has been seen

for stars in dense clouds. Cardelli et al. (1989) have presented a parameterized form of the extinction law as a function of $R_V = A_V/E(B-V)$. Values of R_V up to 5.6 have been seen for stars in the star forming regions in Orion (see e.g. Cardelli et al. 1989). Another possible effect is the scattering of the light by dust grains. If the stellar source we observe is not actually the star, but instead a reflection of the star off dust clouds, then the emission will be altered by a scattering law, λ^{-4}. Finally, the presence of a veiling continuum may contribute a blue component to the stellar flux. A veiling continuum could, for example, be due to hot gas at the accretion disk boundary layer, and is frequently used as a measure of the accretion activity in T Tauri stars (e.g., Hartmann & Kenyon 1990; Batalha & Basri 1993). We compared our observed spectrum with models including all of these effects. We started with the best model with normal extinction, no veiling, and no scattering, and slowly added additional effects to judge the importance. We hoped to constrain the possible range of R_V values, to determine roughly the amount of veiling, and to test if a reflected model may be discriminated from a direct image model on the basis of just the continuum shape.

We first attempted to add a significant veiling continuum, in an attempt to make the model and observations agree for $\lambda < 4300$Å, where there is a clear excess for the simplest model. One constraint on the amount of veiling is independent of the continuum shape: it is not possible to add a large veiling continuum without reducing the strength of the absorption lines too much. The G-band is particularly sensitive to this effect, as it is a significant, deep line in the blue, but the Fe I lines at $\lambda > 5000$ also show this effect. For comparison with Hartmann & Kenyon (1990), we determined the strength of the veiling continuum by measuring the flux ratio $r = F_{veil}/F_{star}$ at 5200Å. When $r > 0.1$, the G-band is somewhat reduced, for $r = 0.25$, the G-band is no longer deep enough, but the other redder lines are still acceptable, and at $r = 0.5$ all of the Fe I lines are too weak compared with the observations. With an optically thick continuum ($\tau > 1.0$), it is not possible to add enough veiling emission to explain the blue emission at $\lambda < 4300$Å without completely washing out the absorption lines. As the veiling emission becomes more optically thin, the ratio of the Balmer emission lines to the continuum increases. In this case, a large fraction of the blue emission may be explained by blended Balmer lines. A model with $r = 0.25$ and $\tau = 0.22$ agrees with the Balmer line flux in the blue region, as well as with the observed Hγ and Hβ line fluxes, but it does not explain all of the observed flux in the blue region. If the optical depth of this veiling is decreased much below 0.2, too much flux is produced in Hβ to allow the veiling to explain the blue emission. We conclude that the level of veiling is $r < 0.25$, due to a marginally optically thin gas, and that, while some of the excess emission seen in the range $\lambda < 4300$Å may be due to Balmer line emission, much of it must be due to a variety of other emission lines, to photometric uncertainty or to calibration errors at the edges of the spectrum.

The value of R_V is not strongly constrained by the shape of the spectrum in this relatively narrow spectral region. It is possible to increase the R_V value and still achieve acceptable fits by simultaneously increasing the extinction. There are small changes in the shape of the continuum, but for the range $2.5 < R_V < 4.5$ the models are acceptable. When R_V is too low, the region 4800Å $< \lambda <$ 6000Å has too much flux in the model, and when R_V is too high, this region has too little flux. A difficulty in determining the value of R_V is the clear presence of a blue excess and the possible presence of a near-IR excess from circumstellar material. We are unable to use the photometry beyond R to improve the constraint of R_V because these bands may be contaminated by emission from a circumstellar disk. While the best value of R_V is roughly 3.1, we cannot rule out values in the range $2.5 < R_V < 4.5$.

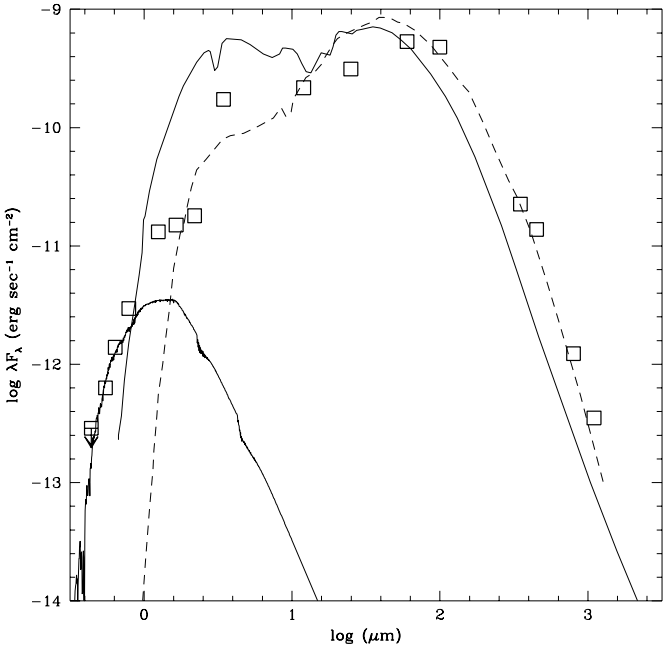

Fig. 2. Spectral Energy Distribution for IRAS 05327+3404 (Holoea). The thick solid line is a stellar spectrum with temperature 4750 K and extinction $A_V = 2.3$ for comparison with the observations. The thin solid line is the best Calvet et al. (1994) model. The dashed curve is the best model from Adams & Shu (1986). See Table fluxes for photometry values.

All of the above conclusions assume we see the star directly. If the flux we see is the result of scattering, we must adjust the spectral shape by λ^{-4} (see e.g., Whittet 1992). It is not possible to find an acceptable fit with normal extinction and scattering. However, by including anomalous extinction, it is possible to find an acceptable fit. The best scattering model has $R_V = 5.0$ and $A_V = 8.5$, using the K2 III spectral template. As before, we can decrease R_V if we decrease the value of A_V. Acceptable fits are found for the range $4.0 < R_V < 6.0$. The best fit with scattered emission and anomalous extinction is essentially indistinguishable from the best model without scattered emission. We conclude that it is not possible to distinguish the scattering model and direct model on the basis of the spectral continuum shape alone, though Occam's razor would suggest the simplest model is favorable. Below, we will discuss the arguments in favor and against the scattered light model.

3.2. Spectral energy distribution

In Fig. 2, we show the broadband spectral energy distribution for the central source from 0.45 μm to 1100 μm, based on the IRAS data and our broadband photometry. The fluxes for the central source at wavelengths longer than L include the JCMT observations reported above and the IRAS observations. These points, especially the IRAS points, should be viewed with some care because of the large beam size. As noted above, there is evidence in our 800 μm data of some extended emission at these wavelengths. However, the fact that the IRAS source does not appear extended in the deconvolved image suggests that the level of contamination is small. Also, there is evidence at other wavelengths of only a limited number of other young stars in the area, all substantially fainter than Holoea at 3.6 μm.

The spectral energy distribution (SED) shows a peak around 60 – 100 μm, a non-thermal distribution on the blue side of the peak, and a submillimeter spectral shape of $\nu F_\nu \sim \nu^\alpha$ where α is in the range 3.5 – 4. The submillimeter spectral index of 3.5 – 4 may be understood in terms of a thermal spectrum from dust grains with an emissivity proportional to ν^β, where $\beta = \alpha - 3$. The range 0.5 – 1.0 for β is typical for dust in the submillimeter (e.g., Whittet 1992; Beckwith & Sargent 1991). The peak of the spectrum shows that the coolest emission components have a temperature around 25K. The SED between 100 μm and 3 μm has a slope which is typical of flat spectrum sources (see e.g. Calvet et al. 1994). The flux in the optical bands principally represents emission from the photosphere of the central star, with some moderate absorption ($A_V \sim 2.3$; see discussion above). For comparison, we have included in the figure a model spectrum (Kurucz 1991) for a star with a temperature of 4750 K and an extinction of $A_V = 2.3$. The flux in the near IR (J, H, K) represents emission from a warm component in excess of the stellar photosphere. The measured nbL flux is surprisingly high, especially when compared with K. It is unlikely that this is due to variability, as the nbL image was taken within minutes of the *JHK* images. We have no explanation for the extreme $K - nbL$ color.

Several groups have made models of the expected SED of YSOs at various stages in their evolution. Models by Adams & Shu (1986) include an extended dust envelope, a central protostar, and an active accretion disk, which means that the energy generated through viscosity in the disk raises the temperature of the disk. The thermal structure of the accretion disk and the temperature of the central source are fixed by the accretion rate and the processing efficiencies, while the thermal structure of the envelope is calculated based on the resulting star + disk luminosity. In models by Calvet et al. (1994), the central disk is passive, which means it does not generate its own heat. In this case, the disk thermal structure is determined by the reprocessing of the stellar radiation field. Both of these groups present models with various choices for the free parameters.

We have compared the observed SED of IRAS 05327+3404 (Holoea) with the models of these two groups. We find that none of the models are able to describe the entire SED particularly well. Of the Calvet et al. models, those which are most successful have viewing angles nearly pole-on, or large values of the centrifugal radius (implying high rotation rates). However, if the viewing angle and opening angle of the central hole are chosen to give sufficient optical emission, then the near or mid IR regions have much too little flux. The best of the Calvet et al. models is shown in Fig. 2 as a solid curve. This has parameters $\rho_1 = 3 \times 10^{-14}$ g cm^{-2}, $R_c = 200$ AU, $\theta = 5°$, and $i = 30°$, and is shown in their Fig. 6. Of the models by Adams & Shu (1986), the best comparison is a model with the highest rotation rate, shown as a dashed line in the figure. This model has parameters of $M = 0.5 \mathrm{M}_\odot$, $a = 0.2$ km s^{-1}, $\eta_D = 1$, $\eta_* = 0.5$, and $\Omega = 3 \times 10^{-14}$ rad s^{-1} and is shown in their Fig. 6. Adams & Shu point out that higher rotation rates make the general shape of the SED wider by allowing a better view of the central source while maintaining large amounts of cool material at large radii. Thus, both sets of models suggest that a high cloud rotation rate is necessary to explain the width of the observed SED.

There is a possible alternative explanation for the combination of the large far-IR flux and the optically visible central star: the system may be a binary star, in which a still-enshrouded star is the source of the far-IR flux. There are a small number of systems consisting of a T Tauri star and an embedded infrared companion. Konesko et al. (1997) discuss the evolutionary status of this class of systems. If this is the case for Holoea, there is a natural dividing line in the SED: the flux from L to the submillimeter would be due to the embedded star while the flux from the optical to K would be due to the optically visible star. However, the L-band image shows a point source which is coincident with the optical and near-IR stellar source to within 0$''$.1, the accuracy of the alignment of the images. Second, there is other evidence for the necessary circumstellar material with a wide central hole, as implied by the SED models. This evidence comes from the morphology of the reflection nebula, and is discussed below.

Even if Holoea is not a binary, we are hesitant to draw very strong conclusions about the properties of the circumstellar material present in Holoea on the basis of the model comparisons. The models produce SEDs which agree with observed SEDs in a general sense, but are probably still too simplified to predict details. Current models all make simplifying assumptions to reduce the computational difficulty of the modelling problem. For example, they invoke spherical symmetry to avoid a 3-D radiative transfer problem. Certain of the models by Calvet et al. (1994) break the spherical symmetry by including a central hole, but these are calculated under the assumption of spherical symmetry, with a correction for the additional heating on the conical surface of the hole due to the central star. The authors offer warnings about the approximations involved, which we will heed. Before strong conclusions can be made about the geometry of the system, more detailed, 3-D radiative transfer models are necessary. However, we can draw some conclusions: First, the central source suffers only moderate extinction, implying that we are looking along a central hole of some kind, though as we discussed above, it is possible that we are seeing the central star via a reflection down the central hole. Second, the large amount of emission in the far IR suggests that large

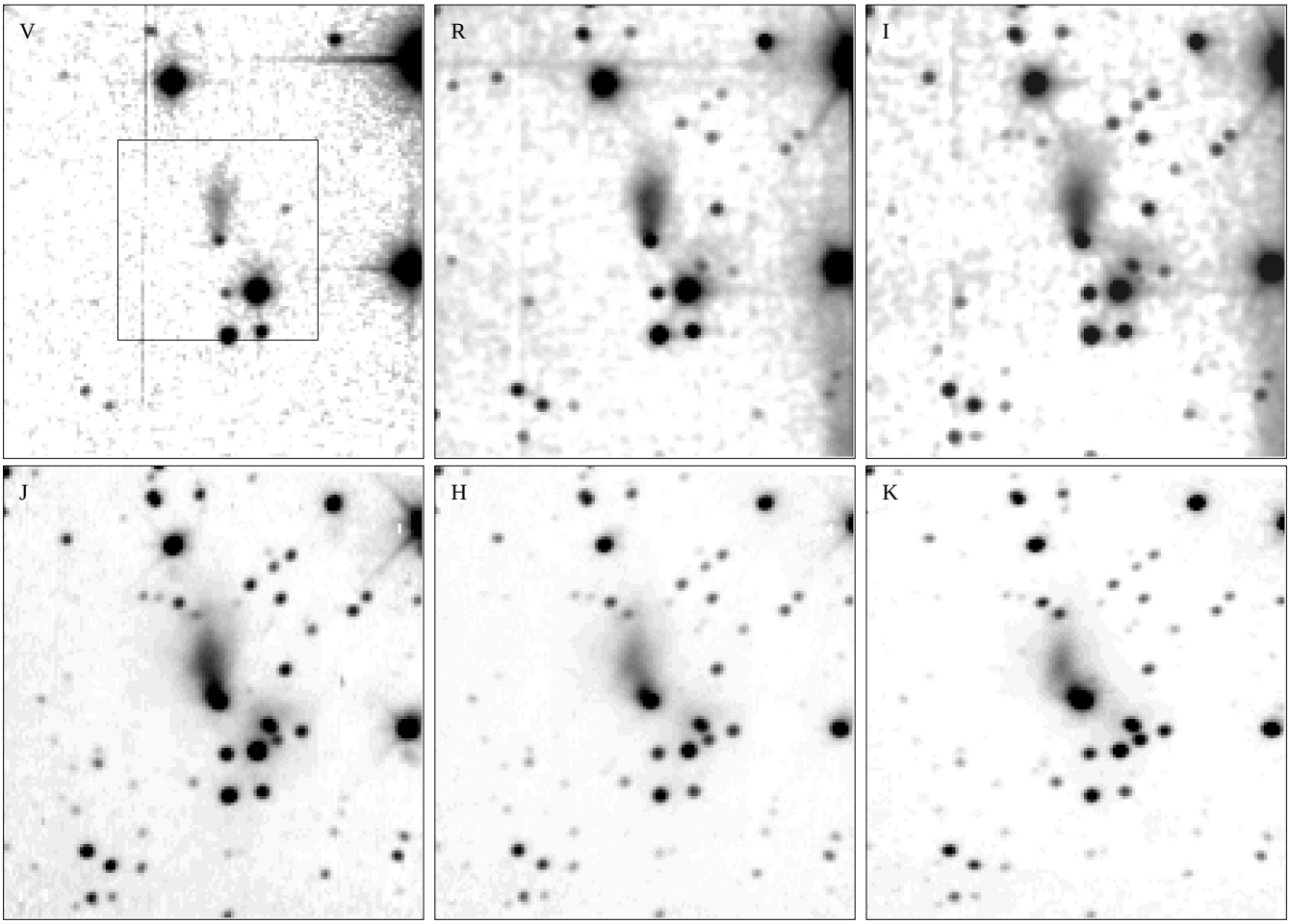

Fig. 3. V, R, I (top left to right) and J, H, K (bottom left to right) images of IRAS 05327+3404 (Holoea). The small inset box in the V image shows the region covered in Fig. 4. These images are each $90'' \times 90''$, with North up, East left.

amounts of dust surround the source at a large distance, corresponding to the outer extremities of the circumstellar disk or to a large circumstellar envelope. Finally, the high level of mid-IR emission suggests the presence of warm circumstellar material on a smaller scale, presumably an accretion disk or the remnant material of an accretion disk. We are hesitant to use the term accretion disk since the small amount of veiling seen in the optical spectrum (see above) suggests that the current accretion activity is fairly small.

4. The reflection nebula

Fig. 3 shows a series of images of Holoea in 6 different bandpasses, V, R, I, J, H, and K. There is a clear variation of the morphology of the reflection nebula as a function of the filter central wavelength. We will now show that all of the morphology observed in these images can be understood in terms of a combination of scattering and obscuration. Furthermore, we can use the reflection nebula to probe the distribution of material near the central star.

4.1. Scattered light model

First, we make the assumption that the bulk of the light from the central source is coming to us directly from the central star, with some amount of extinction by intervening dust, but without scattering: i.e., we can see the central source directly. We will justify this assumption in more detail below. Thus, the observed flux from the central star is:

$$f_\star(\lambda) = f_{\star,0}(\lambda) 10^{-0.4 A_{V,1} \frac{A_\lambda}{A_V}} \quad (1)$$

where $f_\star$ is the observed flux of the central star, $f_{\star,0}$ is the unextinguished flux of the central star, $A_{V,1}$ is the extinction to the central star along the direct line of sight, and $\frac{A_\lambda}{A_V}$ is the extinction law. We assume the canonical extinction law, with $E(B-V) = 3.1 A_V$ (i.e., Cardelli et al. 1989). Next, we assume that the light we observe from the reflection nebula is the result of scattered light from the central star. The flux we observe therefore has both the effects of extinction as well as scattering:

$$f_{neb}(\lambda) = f_{\star,0}(\lambda) 10^{-0.4 A_{V,2} (\frac{A_\lambda}{A_V})} \Gamma (\frac{\lambda}{\lambda_o})^{-\gamma} \quad (2)$$

Where $f_{neb}(\lambda)$ is the observed flux from a point in the reflection nebula, $A_{V,2}$ is the total extinction along a path from the central

star, reflected off the nebula, and towards us, Γ is a normalization factor to determine how much light is scattered by the dust particles in the nebula, and γ is the slope of the scattering function. For Rayleigh scattering, $\gamma = 4$, and for most other types of scattering, γ is still quite close to 4 (Whittet 1992). We do not include the effect of an anomalous extinction law for two reasons. First, as discussed above, the optical spectrum is most consistent with the nominal R_V value of 3.1. Second, and more importantly, changing the value of R_V has a more significant effect on the shape of the ultraviolet extinction, and only a small effect in the near IR. Any anomalous extinction behavior will make a small shift in the level of observed extinction, but should not significantly alter the derived morphology.

If we take the ratio of the flux from any location in the reflection nebula to that of the central star, we can remove the uncertainty in the intrinsic spectrum of the central star:

$$\frac{f_{neb}}{f_\star} = 10^{-0.4(A_{V,2}-A_{V,1})\frac{A_\lambda}{A_V}} \Gamma (\frac{\lambda}{\lambda_o})^{-\gamma}. \quad (3)$$

Expressing this in terms of logarithmic fluxes, we find:

$$\log(\frac{f_{neb}}{f_\star}) = -0.4 \Delta A_V \frac{A_\lambda}{A_V} + \log\Gamma - \gamma \log(\frac{\lambda}{\lambda_o}) \quad (4)$$

Thus, by fitting to the flux ratios, we can determine the increased amount of extinction experienced by the light as it travels to different locations in the reflection nebula from the central star, $\Delta A_V \equiv A_{V,2} - A_{V,1}$.

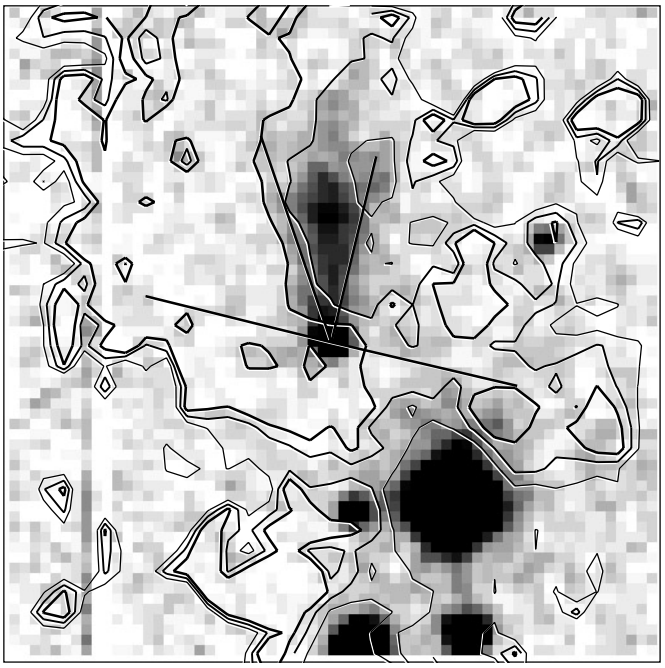

Fig. 4. Map of ΔA_V as a function position in the reflection nebula. The greyscale shows the V image, while the contours show the value of ΔA_V. The values of the contours from thin to thick are 1.5, 3.0, 4.5 magnitudes. The line of sight with the lowest extinction is marked, along with the perpendicular, the assumed orientation of the circumstellar disk. A third line shows the direction towards $\Delta A_V = 4.0$, at roughly 33°.

4.2. Analysis of the images

To perform this measurement, we have rotated and scaled the images to match each other, so that the same pixel in each image represents the same point in the sky. We have also smoothed the images with Gaussian profiles to give them matching PSFs. Finally, we rebinned the images to a fairly large pixel scale (0.″69 per pixel) to increase the signal-to-noise in the nebulosity. The resulting images are shown in Fig. 4. For each of the resulting images, we have subtracted the sky level and converted the fluxes in each pixel to Janskys. We used the photometric calibrations to determine a relationship between pixel counts and magnitudes, and used the conversion factors listed in Landolt-Börenstein (1982) to go from magnitudes to flux units.

The values of ΔA_V and $\log\Gamma$ at any location in the image are given by Eq. 4. We can solve for ΔA_V and $\log\Gamma$ as a function of position by performing a linear least-squares fit of this equation to the fluxes from any pixel in the six images. This fit is done on a pixel-by-pixel basis, fitting the model to the six spectral channels. For the values of $f_\star$, we used our photometric measurements (see Table 1). These flux measurements introduce one of our largest sources of error, the other large source being photon statistics, particularly for the V band image. Fig. 4 shows a contour map of ΔA_V for the field of Holoea derived from these fits. This figure includes only the inner portion of the images in Fig. 3; a box in Fig. 3 shows the limits of Fig. 4. We have overlayed the contour plot of ΔA_V on the V band image for comparison. The reduced χ^2 values are quite reasonable ($\sim$1) in the regions of significant emission from the reflection nebula. At the location of other stars, where our model for the flux is clearly inappropriate (since the dominant source of flux is another star), the χ^2 values are quite high. These χ^2 values imply that our model is a reasonable description for the flux observed from the reflection nebula.

The regions with the lowest extinction are found along the optical tail, and slightly to the west. The extinction increases gradually as the line of sight from the star to the nebula tilts towards the east and, at a lesser significance level, to the west. This pattern of extinction is consistent with our general picture of the system. We know from previous work (Paper I) that there is an ionized outflow which travels roughly towards the optical tail in the north, and which is evident in the P Cygni profile seen in the spectrum reflected by the tail. We also showed in Paper I that there is the suggestion of a circumstellar disk evident in the shape of the [O II] lines, which exhibit extensive blue-shifted emission, but no redshifted emission. We expect the ionized outflow to be oriented perpendicular to the circumstellar disk. The extinction pattern is also suggestive of a circumstellar disk which causes the regions towards the east and west to view the star though an extensive amount of material, while the regions towards the north have a line of sight which is more nearly clear of material.

The map of extinction gives us some interesting details about the distribution of the circumstellar material. First of all, the an-

gle between the region of lowest extinction and the region where the extinction climbs significantly tells us the opening angle of the hole in the circumstellar material. We have measured the angle to be $\sim$33°, between the axis of lowest extinction and the line shown in Fig. 4 where ΔA_V rises to 4.0. We know from the high-resolution optical spectra discussed in Paper I that the angle between the reflected view of the ionized outflow (which is roughly down the path of the outflow) and the direct view is $\sim$ 45°. The agreement between these measurements is reassuring. There are two other aspects of the jet and polar hole geometry to note. First, the angle between the region of lowest extinction and the region of reflection in which the outflow P Cygni profile is observed (Paper I) is $\sim$11°. This angle is a measurement of the collimation of the jet: if we assume the outflow is aligned with the region of lowest extinction, then 11° is roughly the half-width of the outflow cone. Finally, we note that even the region of lowest extinction has a *positive* value of ΔA_V. This suggests that the direct image of the central source has the lowest extinction of any of the lines of sight evident in this image. However, this does not imply that the direct line of sight has the lowest extinction of *all* lines of sight. It is quite possible that the region directly above the pole, where the lowest extinction is naturally expected, also has very little dust to cause a reflection. Thus, the flux that we see in the region of lowest extinction in Fig. 4 comes from the front or back side of a conical distribution of reflecting dust.

An interesting result of these fits is that the asymmetry seen in the reflection nebula need not imply an asymmetric distribution of the circumstellar material. Rather, the asymmetry is due to variations in the amount of dust at a large distance from the star which is available for the scattering process. The extinction map represents the nearby amounts of circumstellar material, which appears to have general axial symmetry, with higher levels of extinction on both the sides of the direction of the outflow. The observed level of extinction on the West side of the star is somewhat lower than on the East, but the flux in this region is quite low, with a correspondingly higher level of uncertainty. We assume the dust causing the scattering is much further from the star than the material causing the extinction. At a distance of $\sim$10,000 AU ($\sim$10″) from the star, it is perhaps left over from the original cloud.

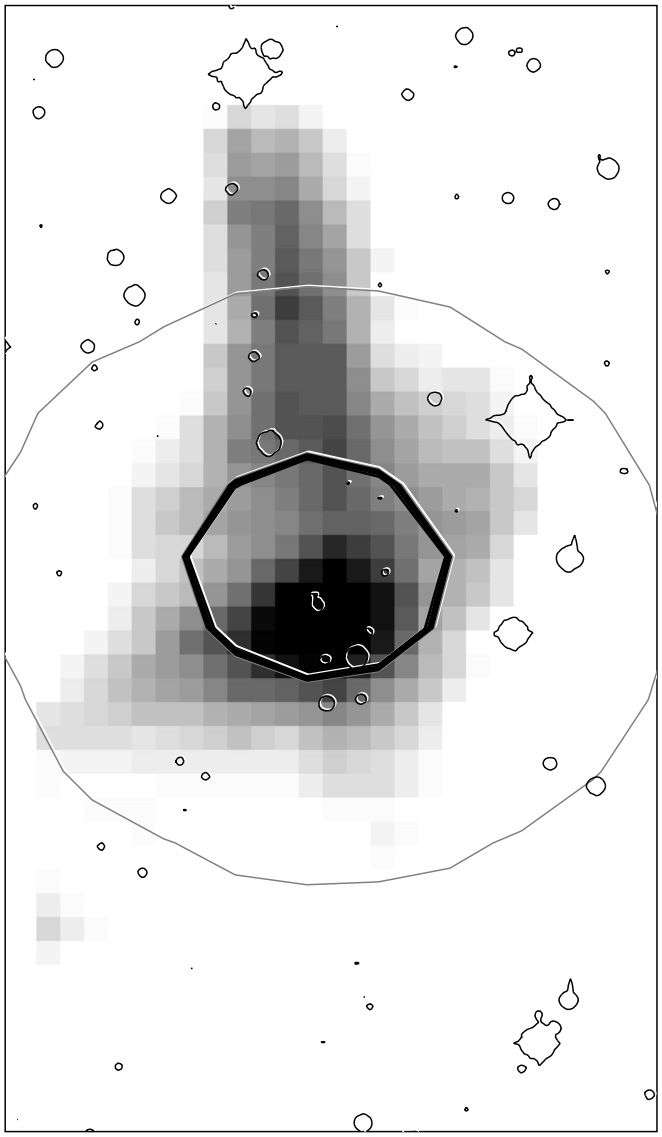

Fig. 5. Integrated CO J = 2-1 map. The CO emission is integrated from V_{LSR} $-$14.5 – $-$34.7 km s^{-1} and is shown in grey scale for the range 15 – 40 K km s^{-1}. The thin black contours are from the V band image. The thick black and thin grey contours are the IRAS 60 μm flux densities. Holoea lies directly at the center of the IRAS source. This image is 3.′6 × 6.′3, North up, East left.

4.3. Direct image or reflection?

One of the assumptions employed in the analysis above was that the central source represents light coming directly from the central star with some extinction, but without scattering. We will now present evidence to support this assumption.

First, the location of the stellar source does not change position with wavelength. In some other systems, such as L1551-IRS5, there is a bright stellar source which, on closer inspection, is found to be a bright reflection of a more embedded source (see e.g., Staude & Elsässer 1993, for an extensive review). However, in cases such as this, the location of the bright stellar source changes with wavelength as different portions of the reflection nebula are seen. The location of the stellar source seen at V though L are coincident to within 0.″1, as discussed above. Second, the flux from the reflection nebula is well modeled as the flux of the central source adjusted for extinction along the line of sight and scattering towards us. It is not possible to model the stellar source and the nebula as having only different amounts of extinction. If the central source resulted from scattered light, then the reflection nebula would have to be the result of *two* scatterings to be consistent with the spectral fits. This seems to be quite implausible, and a very unusual geometry would be required to account not only for the observed distribution of nebulosity, but also for the Hα line profiles observed in the high-resolution spectra reported in Paper I. Finally, the spectrum of the central source is well represented by a stellar

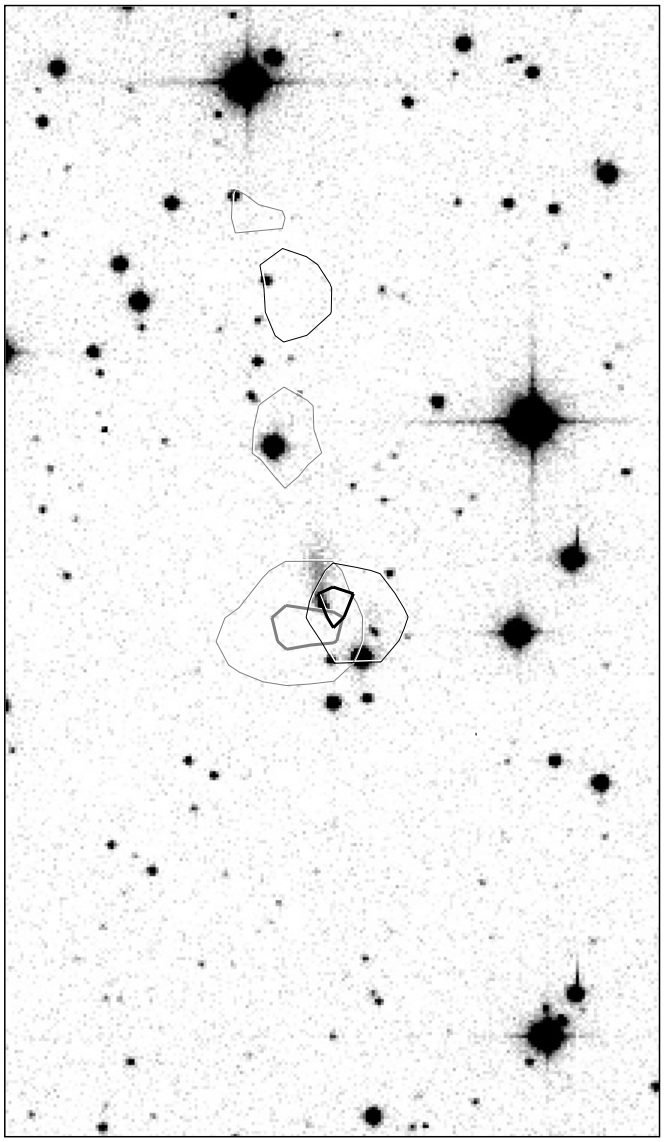

Fig. 6. CO J = 2–1 velocity contours overlayed on a V image. The grey lines are redshifted CO emission, while the black lines are blue-shifted CO emission. In both cases, the thick lines have a high velocity relative to the system and the thin lines have a low relative velocity. Table 3 gives the exact velocity ranges and flux levels for the contours. Same scale as Fig. 5.

spectrum modified by extinction. To incorporate a scattering term requires introducing a large extinction (8.5 mag) and an anomalous R_V value of 5.0. Occam's razor argues in favor of the simpler model: no scattering and no anomalous extinction. On the other hand, it is easier to explain the ratio of Hα to Hβ with the level of extinction needed in the scattered light model. However, since the Hβ flux is not very well measured in our spectrum, and since the Hα emission is clearly from a non-LTE source, this does not give strong support for the scattered light model. We conclude that the simplest model has a direct view of the central source as a result of a wide opening angle in the circumstellar material. The interpretation is consistent with the extinction pattern observed in Fig. 4 as well as the observed emission line profiles.

5. The molecular outflow

Fig. 5 shows a map of the integrated CO flux in the vicinity of Holoea. We have also included contours of the V image, to show the location of the stars and the IRAS 60 μm image, deconvolved using the Groningen HIRAS routine (Bontekoe et al., 1994). The heavy IRAS contour is chosen to mark the FWHM of the IRAS source, while the thin IRAS contour is close to the sky level and shows the outer limits of this IRAS point source. The brightest CO feature in the map is coincident with the location of Holoea, but fainter extended emission is seen in a region of $2' \times 4'$. The CO emission in the vicinity of Holoea has the largest velocity dispersion, as well as the strongest emission. The bright CO source associated with Holoea is clearly associated with a larger, fainter CO cloud.

Fig. 6 shows the V image with contours from redshifted and blue-shifted CO maps. The grey contours show the redshifted components, while the black contours show the blue-shifted ones. For both red and blue-shifted contours, the heavy contours have a high velocity relative to the system rest velocity, while the light contours have a low relative velocity. The velocity ranges and the flux levels for the contours are listed in Table 3. In the immediate vicinity of Holoea, there is a pattern suggestive of a bipolar outflow: the red and blue-shifted contours are displaced to opposite sides of the central star. The direction of the outflow appears to be in roughly the same direction as the direction of the lowest extinction seen in Sect. 4, generally West of North.

6. IRAS 05327+3404 (Holoea) in an evolutionary context

The evolutionary status of Holoea is something of a puzzle. It is clearly a young stellar object of some type, given the spectral energy distribution and the existence of molecular and ionized outflows. However, several of the observed features appear to lead towards contradictory conclusions. The central star is observed directly with only a minimal amount of extinction ($A_V \sim 2.3$ mag), as would be expected in a fairly evolved pre-main sequence star. But, there is the strong far-IR emission and CO outflows typically seen in more embedded systems. As we discussed above, there is the possibility that the optically visible star is either a reflection or a binary system. While either of the two possibilities would make it easier to understand the SED, we have presented arguments why they are unlikely for other reasons.

As mentioned in Paper I, the central star of Holoea has become brighter in the last 40 years. On red POSS plate of this field taken Nov 11, 1954, the central star is barely visible (Fig. 7). A comparison with other stars in the field shows that the central star at the time of our first observations on October 2, 1993, the central star has brightened by $\gtrsim$1.5 mag (see Fig. 7). We have ruled out a color effect, as stars with colors similar to that of Holoea do not appear substantially fainter on the POSS plate image. The POSS II survey also observed this field Oct 4, 1989. In

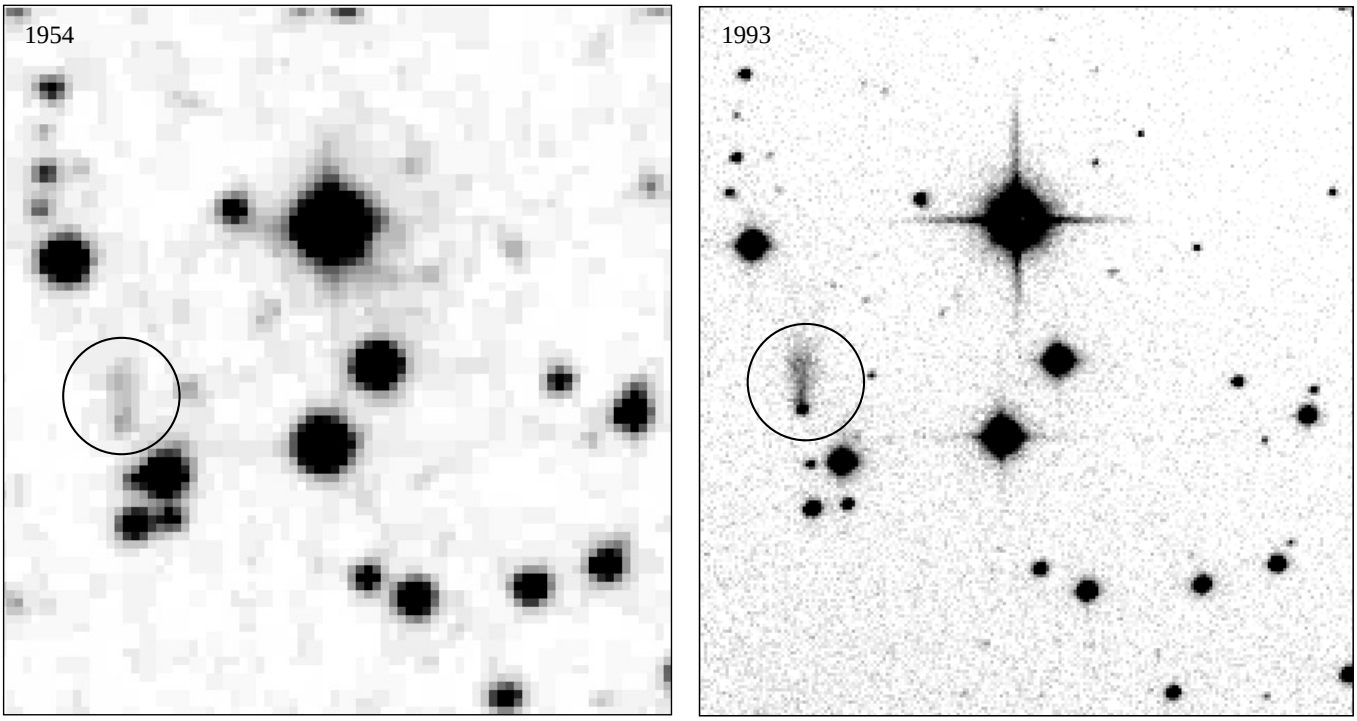

Fig. 7. This figure shows the 1954 red POSS plate and 1993 R CCD images of Holoea (circled). Holoea has brightened substantially between these two images.

Table 3. CO contour levels in Fig. 6

contour	V_{LSR} range (km s^{-1})	flux (K km s^{-1})
thick grey	-14.7 – -15.5	1.0
thin grey	-17.5 – -18.3	1.4
thin black	-24.2 – -25.0	1.4
thick black	-30.3 – -31.1	0.5
$\sigma_V = 0.1$ K km s^{-1}		
V_{LSR} of peak flux at central star = -21.1 km s^{-1}		

the red POSS II image, the central star appears to already have reached the level of the Oct 1993 observations. Observations since Oct 1993 have shown no further evidence of variability.

Several types of young stellar objects show variability. Many T Tauri stars exhibit small levels of stochastic variability which may be due to changing accretion rates or changing amounts of obscuration. FU Orionis (FUor) systems show outbursts characterized by sudden, large increases and slow decreases in their brightness, thought to be the result of large, short-lived accretion events. EXor systems usually show smaller, shorter outbursts, which may be due to a similar mechanism to the one responsible for FUor outbursts (Lehmann et al. 1995). This class is named for the star EX Lupi, and invokes the similarity with the FUors. However, the observed brightening of Holoea does not seem to be consistent with either of these types of variability. The increase seems to have been a single change, as there is now no evidence of variability or the slow decay seen in FUors. In the case of the FUor and EXor systems, the increase in brightness is associated with an increase in the flux from the accretion disk. For EXors, which have a strong UV excess and strong high-Balmer lines, the increase in the veiling continuum accounts for most of the increase in flux (Lehmann et al. 1995). Since the veiling in Holoea is now only $\lesssim$25%, this could not be responsible for a 1.5 mag increase in brightness. In the case of FUors, the accretion rate is so high that the boundary expands and takes on the spectral characteristics of a late F or G type star. The brightness increase is attributed to this increased emission (Hartmann & Kenyon 1996). However, our spectra show that the flux at R from Holoea is dominated by a stellar photosphere of spectral type early K. If this is the emission from an extended boundary layer, it is quite cool compared to those of FUors.

An alternative mechanism by which the central star may have gotten brighter is if the amount of extinction has decreased. In Paper I, we suggested that Holoea represents a transitory phase in the evolution of low-mass YSOs from the embedded to the exposed phases, also called Class I and Class II T Tauri stars (Lada & Wilking 1984). This suggestion was based principally on the combination of a visible central source and a flat spectral energy distribution. Given the presence of strong outflows, seen in both ionized and molecular gas, the observed increase in brightness could be the result of clearing of the polar holes.

It would have been interesting to trace the process by which a YSO clears out the central regions if we could have followed the increase in the brightness of the central source since 1954, when the POSS plate was taken. We have searched the Harvard plate stack library for any observations in the intervening 40 years, but without success. Given the V magnitude of 18.6 and

the crowded field, only very deep and large-scale photographic plates could have detected Holoea. None of the existing Harvard plate stack images of the region are both deep enough and have high enough spatial resolution. We have also searched the literature for observations, particularly of M 36, since Holoea is within the field of the cluster. Several old photographs of M 36 exist, and these were used for measuring the proper motion (Hagen 1970). However, the only one taken after the POSS plate image was from fall 1954 (Bronnikova 1958), at roughly the same time as the POSS plate image. Unless unpublished observations of M 36 exist in other plate archives, it is unlikely that we will obtain additional, detailed information on the long-term lightcurve of Holoea.

Even if the brightening of Holoea is due to the clearing of the central hole, the evolutionary status of the object is not certain. Our attempts to compare the SED to models suggest that the unusually wide SED is not the result of evolution but rather to the large angular momentum of the circumstellar material. In Sect. 5, we showed that Holoea is part of a very small cloud with only a small number of other possible nearby stars being formed. This small cloud is on or somewhat beyond the periphery of the Taurus-Auriga complex. Lada et al. (1993) discuss the Taurus-Auriga complex and the Rho Ophiuchus complex, and point out that in the first, star formation is taking place in low concentration regions, while in the second the star formation occurs in dense clusters. They also show that the dense, clustered mode of star formation is apparently more common, at least in our part of the Galaxy. Holoea is isolated even compared with the typical star in the Taurus-Auriga complex. We hypothesize that the relative isolation of Holoea compared to the bulk of young stars may be related to the unusually wide SED, perhaps by allowing the formation of large circumstellar disks with high angular momentum which would otherwise be disrupted. It is conceivable that such a high mass, high angular momentum disk may survive much longer than a low angular momentum disk, as the rotation inhibits accretion of the circumstellar material onto the star. This would give the central star time to evolve while the cloud is retained. These last points are speculative, but provide a starting point to consider the differences between stars with different SEDs and apparently similar evolutionary states.

7. Conclusions

We have obtained new observations of the unusual young stellar object, IRAS 05327+3404 (Holoea). We have shown that the central star is directly visible, with only a modest amount of extinction ($A_V \sim 2.3$ mag). The spectral type of the central star is roughly K 2. The spectral energy distribution implies the presence of substantial circumstellar material, and model comparisons suggest the original cloud had significant angular momentum ($\gtrsim 10^{-13}$ rad s^{-1}). A detailed study of the flux detected from the reflection nebula also shows the presence of circumstellar material arranged in an equatorial plane, with a 33° wide polar hole. CO mapping shows the presence of a bipolar molecular outflow aligned with the polar hole (P.A. $\sim -15°$) seen via the reflection nebula. This is roughly the same direction as the ionized outflow evident in the Hα line profiles. The CO map also shows a small ($\sim$0.3 pc) enveloping molecular cloud, and the possible presence of a single, weaker CO outflow. Although IRAS 05327+3404 (Holoea) drives an ionized outflow which is surprisingly fast for a low-mass young stellar object ($\sim$650 km s^{-1}), there is little or no evidence for active accretion in the form of strong UV excess, veiling, or high-Balmer line emission. This suggests that an ionized outflow may exist without the simultaneous presence of a hot, active accretion disk. Two possibilities exist: 1) the observed ionized outflow in Holoea was driven by a hot accretion disk in the recent past which has subsequently shut off, leaving behind the fast-moving jet or 2) the observed ionized outflow is currently being driven, not by a hot accretion disk, but by some other component, such as the cool circumsellar disk or the stellar photosphere. The central star has brightened in the past 40 years, but this brightening does not seem to be due to an increase in accretion activity. We suggest that the brightening is due to reduced extinction as the polar regions are cleared. The unusual presence of a massive circumstellar disk, as seen in the far-IR emission, and a visible central star may imply a large angular velocity for the birth cloud. We suggest that the relative isolation of IRAS 05327+3404 (Holoea) during its formation may have allowed a large amount of material to be maintained in a circumstellar disk with high angular momentum. In addition to having a large circumstellar disk, and few nearby neighbors to disrupt the disk, the large angular momentum may inhibit further accretion, and may allow the circumstellar disk to remain longer than in less isolated systems. Thus, the environment may play an important role in determining the evolution of the spectral energy distribution.

Acknowledgements. This paper is partly based on observations made with the INT, operated on the island of La Palma by the Royal Greenwich Observatory in the Spanish Observatorio del Roque de los Muchachos of the Instituto de Astrofísica de Canarias. Observations discussed in this paper were also performed at the Michigan – Dartmouth – MIT (MDM) Observatory and at the Joint Astronomy Center. We gratefully thank the observers at both UKIRT and JCMT for their assistance, particularly Goeran Sandell and Remo Tilanus. EAM acknowledges support by the Netherlands Foundation for Research in Astronomy (ASTRON) with financial aid from the Netherlands Organization for Scientific Research (NWO) under contract number 782-376-011. Support for EAM was also provided by NASA through grant number GO-06459.01-95A from the Space Telescope Science Institute, which is operated by the Association of Universities for research in Astronomy, Inc., under NASA contract NAS5-26555. YJK acknowledges support by the National Science Council of Taiwan under contract number 87-2112-M-003-007. LBFMW acknowledges financial support from the Royal Dutch Academy of Arts and Sciences. The IRAS data were obtained using the IRAS data base server of the Space Research Organisation of the Netherlands (SRON) and the Dutch Expertise Centre for Astronomical Data Processing funded by the Netherlands Organisation for Scientific Research (NWO). We gratefully thank Do Kester and Romke Bontekoe for use of the IRAS-GIPSY system. The IRAS data base server project was also partly funded through the Air Force Office of Scientific Research, grants AFOSR 86-0140 and AFOSR 89-0320. This article uses data from the Digitized Sky Survey, based on photographic data of the National Geographic Society – Palomar

Observatory Sky Survey (NGS-POSS) obtained using the Oschin Telescope on Palomar Mountain. The NGS-POSS was funded by a grant from the National Geographic Society to the California Institute of Technology. The plates were processed into the present compressed digital form with their permission. The Digitized Sky Survey was produced at the Space Telescope Science Institute under US Government grant NAG W-2166.

References

Adams F.C., Shu F.H. 1986, ApJ 308, 836
Batalha C.C., Basri G. 1993, ApJ 412, 363
Beckwith S.V., Sargent A.I. 1991, ApJ 381, 250
Bontekoe Tj.R., Koper E., Kester D.J.M. 1994, A&A 284, 1037
Bronnikova N.M. 1958, Pulkova Trudy 2, 72
Calvet N., Hartmann L.W., Kenyon S.J., Whitney B.A. 1994, ApJ 434, 330
Cardelli J.A., Clayton G.C., Mathis J.S. 1989, ApJ 345, 245
Casali M.M., Hawarden T.G. 1992, JCMT-UKIRT Newsletter, 3, 33.
Hagen G.L. 1970, Publ. David Dunlop Obs., U. Toronto, Toronto, Vol 4
Hartmann L.W., Kenyon S.J. 1990 ApJ 349, 190
Hartmann L.W., Kenyon S.J. 1996 ARA&A 34, 207
Konesko C.D., Herbst T.M., Leihert Ch. 1997, ApJ 480, 741
Kurucz R.L. 1991 IAU Symposium 149 Brazil
Lada C.J., Wilking B.A. 1984, ApJ 287, 610
Lada E.A., Strom K.M., Myers P.C. 1993, 'Protostars and Planets III', University of Arizona Press, Tucson, p. 254
'Landolt-Börenstein: Numerical Data and Functional Relationships in Science and Technology: B Stars and Star Clusters', 1982, Springer, Berlin, eds. Schaifers K., Voigt H.H., Landolt H., Börenstein R., Hellwege K.H.
Lehmann T., Reipurth B., Brandner W. 1995, A&A 300, L9
Magnier E.A., Waters L.B.F.M., Kuan Y.-J., Chu Y.-H., Taylor A.R., Matthews H.E., Martín E.L. 1996, A&A 305 936 (Paper I)
Massey P., Strobel K., Barnes J.V., Anderson E. 1988, ApJ 328, 315
Silva D.R., Cornell, M.E. 1992, ApJS 81, 865
Staude H.J., Elsässer H., 1993, A&AR 5, 165
Whittet D.C.B., 1992, 'Dust in the Galactic Environment', IOP Publishing Ltd., New York